Microdefocusing Method for Measuring Acoustic Properties Using Acoustic Microscope

Hiroshi Kanai, *Member, IEEE,* Noriyoshi Chubachi, *Member, IEEE,* and Toshio Sannomiya

Abstract—**Many papers have been reporting on measurement of acoustic properties of materials by acoustic microscopy. In a conventional method of $V(z)$ curve analysis, the phase velocity and the propagation attenuation of a leaky surface acoustic wave (LSAW) are determined from the interference period Δz and the slope of the $V(z)$ curve, respectively. For this method it is necessary to measure the $V(z)$ curve for a period several times as long as the interference period Δz. Therefore, it is difficult to measure the acoustic properties of a sample with high resolution by the method.In order to overcome these problems, a new method called the *microdefocusing method* is proposed, to determine the acoustic properties of a sample by analyzing $V(z)$ values measured in the microdefocusing region within an interference period Δz near a focal plane. A new-type of ultrasonic transducer called the *butterfly transducer* is proposed to be applied to this microdefocusing method and a digital signal processing procedure is developed to analyze the output of the ultrasonic transducer. Basic experiments are performed to confirm the principles of the new method.**

I. Introduction

THIS PAPER presents a new method to obtain acoustic properties of a sample by analyzing $V(z)$ values measured in the microdefocusing region near a focal point in an acoustic microscope. Since the mechanically scanning acoustic microscope (SAM) was first developed by C. F. Quate *et al.* [1], many papers have been published on acoustic measurement and imaging using acoustic microscopy [2]. Angular spectrum approaches were developed to derive an expression for the contrast mechanism in the imaging of the reflection acoustic microscope using the reflection function [3]. The $V(z)$ curve, which is the transducer output recorded against a distance z from the focal point, has many peaks and dips generated due to the interference of a leaky surface acoustic wave (LSAW) component $V_I(z)$ and a wave component $V_L(z)$ reflected perpendicularly to the surface. The periodicity of the dips appearing in the $V(z)$ curves was analyzed by R. D. Weglein [4]. The models describing the relationship between the dip interval (interference period Δz) and Rayleigh wave velocity were presented by Parmon *et al.* [5] using a ray model and by A. Atalar [6] using the angular spectrum approach [3]. Based on these pioneering works, many acoustic microscopic methods and systems for analyzing the $V(z)$ curves have been developed in the fields of acoustical imaging and quantitative measurements such as [7]. In a conventional method, the phase velocity and the propagation attenuation of the LSAW component are determined from the interference period Δz and the slope η of the $V(z)$ curve, respectively.

For fused-quartz and other samples, the interference period Δz is several times as long as the wave length λ_w in water. In order to detect the interference period Δz from the $V(z)$ curve based on the periodicity analysis [8] such as the fast Fourier transform (FFT) and to determine the slope η of the $\ln|V(z)|$ curve [7], [9], [10], it is necessary to measure the $V(z)$ curve for a period several times as long as the interference period Δz, that is, the maximum width ΔB of the beamspot on a sample must be several tens of times the wavelength λ_w of the longitudinal wave in the water. Therefore, it is difficult to measure the acoustic properties of a sample with high resolution by these present acoustic microscope systems. When the propagation attenuation of a sample is large and/or the velocity value of the LSAW is large, sufficient defocus distance for the periodicity analysis is not available and then it is also difficult to measure the acoustic properties.

Therefore, we have proposed a new method to determine the acoustic properties of a sample from the $V(z)$ values measured in the microdefocusing region near a focal point [11]. We have also proposed a new-type of ultrasonic transducer, the *butterfly transducer,* in which the electrode is divided into two parts. The principle of the microdefocusing method was preliminarily described in [11]. This paper describes the principle in detail and develops a new signal processing method to analyze the two outputs of the electrodes in the butterfly transducer. By analyzing the two output components, both components $V_L(z)$ and $V_I(z)$ are obtained separately. From the resultant components, the acoustic properties of a sample are determined without any periodicity analysis and without measuring the temperature that is generally difficult to obtain accurately.

II. Current $V(z)$ Analysis and Its Problems

Let us consider the simplest case of one LSAW mode. When the sample is brought close to the acoustic lens by a distance $z(z < 0)$ from the focal plane, the transducer output of $V(z)$ detected at the ultrasonic transducer is dominated by two components as shown in Fig. 1; one component $V_L(z)$ is the transducer output due to the acoustic wave propagating along path (#0) normally reflected from the surface of the sample, and the other component $V_I(z)$ is the transducer output associated with the waves propagating along path (#1) due to the LSAW component propagating on the boundary. Thus, the

Manuscript received October 15, 1991; revised and accepted January 27, 1992.

The authors are with the Department of Electrical Engineering, Tohoku University, Aramaki-aza-Aoba, Sendai, 980 Japan.

IEEE Log Number 9200693.

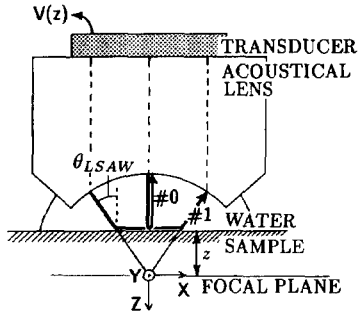

Fig. 1. Cross-sectional geometry of acoustic point-focus-beam lens, which explains the construction mechanism of $V(z)$ curves.

transducer output $V(z)$ is represented by

$$V(z) = V_I(z) + V_L(z). \tag{1}$$

Let us assume that $V(z)$ be sampled at the interval $|\delta z|(\delta z < 0)$, that is, $z = n \cdot \delta z(z < 0)$, where n is the sample number $(n = 0, 1, 2, \cdots)$. Based on references [5], [10], which use ray theory along paths #0 and #1 in water or on the boundary, each of these two components is re-expressed as a damped complex sinusoidal:

$$V_I(n \cdot \delta z) = C_I \cdot p_I^n \tag{2}$$

and

$$V_L(n \cdot \delta z) = C_L \cdot p_L^n \tag{3}$$

where C_L and C_I are the assumed complex constants describing the amplitude and phase characteristics of $V_L(z)$ and $V_I(z)$, respectively, at the focal plane $(z = 0)$. The complex quantities p_I and p_L, which are called "poles" in the research field of digital spectrum estimation, are described by the product of the amplitude term and the phase term as

$$p_I = \exp\left(2\gamma \cdot \delta z \tan\theta_{\mathrm{LSAW}} - \frac{2\alpha_w \cdot \delta z}{\cos\theta_{\mathrm{LSAW}}}\right) \cdot \exp(j2k_w \cos\theta_{\mathrm{LSAW}} \cdot \delta z), \tag{4}$$

$$p_L = \exp(-2\alpha_w \cdot \delta z)\exp(j2k_w \cdot \delta z). \tag{5}$$

The quantities α_w and γ are the normalized attenuation factors for the longitudinal wave in water and for the LSAW, respectively. The quantities k_w, k_{LSAW}, and θ_{LSAW} are the wave number in water, the wave number of the LSAW on the boundary, and the critical angle for the LSAW, respectively. Let quantity v_w be the longitudinal velocity in water and v_{LSAW} be the phase velocity of the LSAW. Then

$$k_w = \frac{2\pi f}{v_w} \tag{6}$$

$$k_{\mathrm{LSAW}} = \frac{2\pi f}{v_{\mathrm{LSAW}}} \tag{7}$$

and

$$\theta_{\mathrm{LSAW}} = \sin^{-1}\left(\frac{v_w}{v_{LSAW}}\right) \tag{8}$$

where f is the ultrasonic frequency.

Due to the interference between $V_L(z)$ and $V_I(z)$, the amplitude curve $|V(z)| = |V_L(z) + V_I(z)|$ has a few dips

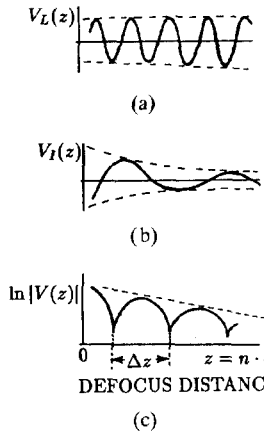

Fig. 2. (a) Real component of the complex $V_I(z)$ of (2). (b) Real component of the complex $V_L(z)$ of (3). (c) Amplitude curve $|V(z)| = |V_L(z) + V_I(z)|$.

in the measured defocusing range as illustrated in Fig. 2. By letting the phase difference between $\angle V_L(z) = 2k_w \cdot \delta_z \cdot n$ and $\angle V_I(z) = 2k_w \cos\theta_{\mathrm{LSAW}} \cdot \delta z \cdot n$ equal 2π, the interference period Δz is described by

$$\Delta z = \frac{\pi}{(1 - \cos\theta_{\mathrm{LSAW}})k_w}. \tag{9}$$

By re-arranging the equation using Snell's law as written in (8), the phase velocity v_{LSAW} of the LSAW is obtained as

$$v_{\mathrm{LSAW}} = \frac{v_w}{\sqrt{1 - (1 - v_w/2f\Delta z)}} \tag{10}$$

where the longitudinal velocity v_w in water is determined beforehand from the relationship [12] between v_w and the measured temperature of water.

In the present system [8], [10], the phase velocity v_{LSAW} of the LSAW is determined from the interference period Δz, which is obtained by applying the FFT on the $|V(z)|$ curve of Fig. 2(c). The attenuation γ of the LSAW is determined from the slope η of the interference amplitude $|V(z)|$ [7], [9], [10], which is shown by a dotted line in Fig. 2(c).

For fused-quartz and other samples, the interference period Δz is usually more than several wave lengths in water. When $v_{\mathrm{LSAW}} \approx 3400$ m/s, $v_w = 1494$ m/s, and $f = 200$ MHz for example, the interference period $\Delta z = 36.7$ μm. From the results of theoretical analysis [13]. there is a large amount in the estimation of the dominant frequency especially when the FFT is applied on the wave that has only about one signal period. Thus, in order to detect the interference period Δz for the $|V(z)|$ curve using the FFT as well as to determine the slope η of the $\ln|V(z)|$ curve, it is necessary to measure the $|V(z)|$ curve at a defocus range of several times the interference period Δz. As a result, the maximum width ΔB of the beam-spot covers a measurement area more than several tens of times the wave length in water to degrade the resolution. Thus, it is difficult to measure the acoustic properties of a sample with a high resolution by the conventional acoustic microscope system.

It is, therefore, necessary to develop an alternative method not depending on the periodicity analysis to determine acoustic properties of the LSAW from the $V(z)$ curves measured in

the microdefocusing range. Such a method is described in Section III.

III. Principle of Microdefocusing Method

From (2) and (3), each of the phase components $\angle V_I(z)$ and $\angle V_L(z)$ and the natural-logarithmic amplitude components $\ln|V_I(z)|$ and $\ln|V_L(z)|$ varies on the straight line as illustrated in Fig. 3. Let their gradients be defined as

$$\xi_I \stackrel{\text{def}}{=} \frac{\partial}{\partial z}\angle V_I(z) = 2k_w \cos\theta_{\text{LSAW}} \tag{11}$$

$$\xi_L \stackrel{\text{def}}{=} \frac{\partial}{\partial z}\angle V_L(z) = 2k_w \tag{12}$$

$$\eta_I \stackrel{\text{def}}{=} \frac{\partial}{\partial z}\ln|V_L(z)| = 2\gamma\tan\theta_{\text{LSAW}} - \frac{2\alpha_w}{\cos\theta_{\text{LSAW}}} \tag{13}$$

$$\eta_L \stackrel{\text{def}}{=} \frac{\partial}{\partial z}\ln|V_L(z)| = -2\alpha_w. \tag{14}$$

Using (8) and (6), the phase velocity v_{LSAW} of the LSAW component is obtained from the gradient ξ_I of (11) by

$$v_{\text{LSAW}} = \frac{v_w}{\sqrt{1-\cos^2\theta_{LSAW}}} = \frac{v_w}{\sqrt{1-(\xi_I v_w/4\pi f)^2}}. \tag{15}$$

Thus, if $V_I(z)$ is obtained separately from $V(z)$ in the defocusing region that is sufficient to measure the gradient ξ_I of $\angle V_I(z)$, the phase velocity v_{LSAW} of the LSAW can be determined by substituting the gradient ξ_I into (15), where the longitudinal velocity v_w in water is obtained from either the relation between temperature and v_w [12] or from the measured gradient ξ_L of $\angle V_L(z)$ in (12) by the relation

$$v_w = \frac{4\pi f}{\xi_L}. \tag{16}$$

In the case where the velocity v_w in water is determined from the measured gradient ξ_L, it is not necessary to measure the temperature of water, which in general is difficult to determine precisely.

The normalized attenuation factor γ for the LSAW is determined from the gradient η_I of $\ln|V_I(z)|$ by using either the relation $\alpha_w/f^2 = 25.3\times10^{-17}s^2/\text{cm}$ [14] or the measured gradient $\eta_L = -2\alpha_w$ in (14). Therefore, both the phase velocity and the attenuation properties of the LSAW component can be obtained from the $V(z)$ curves measured in the microdefocusing region without relying on periodicity analysis methods such as the FFT, if the two complex components $V_I(z)$ and $V_L(z)$ are obtained separately.

IV. A New-Type Ultrasonic Transducer

For the purpose of obtaining the two components $V_L(z)$ and $V_I(z)$ separately, a new type of transducer, which we called a butterfly transducer, is introduced into a conventional point-focus-beam (PFB) lens transducer system as shown in Fig. 4. The transducer is actually composed of three individual parts and is divided into a center transducer and a pair of surrounding transducers. The radius a of the center part and the inner radius b and the outer radius c of the surrounding parts

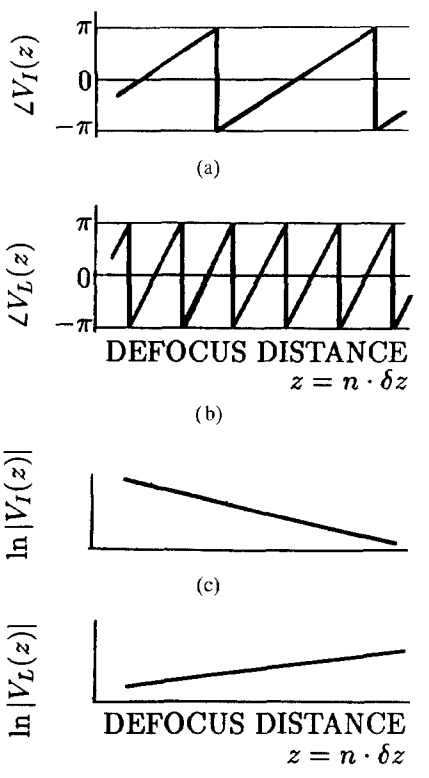

Fig. 3. The phase components $\angle V_I(z)$ and $\angle V_L(z)$ and the amplitude components $\ln|V_I(z)|$ and $\ln|V_L(z)|$

are determined as follows. Let R denote the distance of the path (#1) from the z-axis as shown in Figs. 4 and 5(c-2). By applying Snell's law with respect to point (B) in Fig. 5(c-2), the following relation is obtained.

$$\frac{v_S}{\sin\theta_S} = \frac{v_w}{\sin(\theta_S - \theta_{\text{LSAW}})} \tag{17}$$

where θ_S is the angle between the z-axis and $\overline{OB}$ at the center of curvature (O) and v_S is the longitudinal velocity in the acoustical lens. Using the relation

$$\sin(\theta_S - \theta_{\text{LSAW}}) = \sin\theta_S\cos\theta_{\text{LSAW}} - \cos\theta_S\sin\theta_{\text{LSAW}}$$

$\tan\theta_S$ is described by

$$\tan\theta_S = \frac{v_S\sin\theta_{\text{LSAW}}}{v_S\cos\theta_{\text{LSAW}} - v_w}.$$

From Snell's law given in (8):

$$\tan\theta_S = \frac{v_w}{\sqrt{v_{\text{LSAW}}^2 - v_w^2} - v_w v_{\text{LSAW}}/v_S}. \tag{18}$$

Using the radius r of curvature of the PFB acoustic lens, the distance R is described by

$$R = r\sin\theta_S = r\sin\left[\tan^{-1}\left(\frac{v_w}{\sqrt{v_{\text{LSAW}}^2 - v_w^2} - v_w v_{\text{LSAW}}/v_S}\right)\right]. \tag{19}$$

By taking into account some margin, the radii b and c are

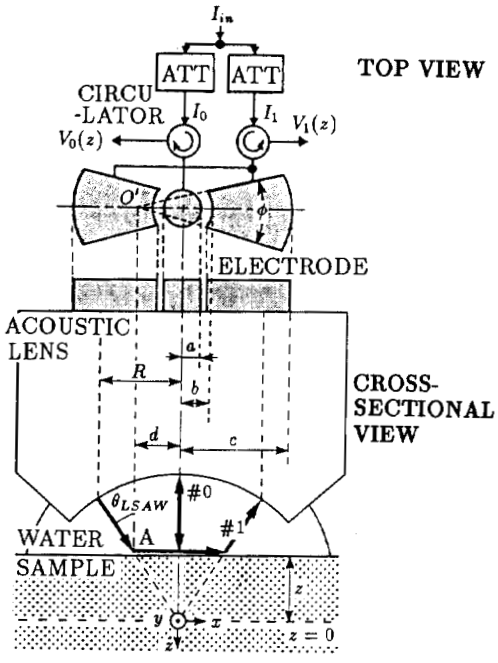

Fig. 4. Cross-sectional and top views of the proposed new-type of butterfly transducer. The electrodes are divided into two parts.

determined from the range of expected v_{LSAW} values of the samples to be measured. The radius a is determined so as to make a as close as possible to b.

For the study of anisotropic materials, several excellent directional transducers have been proposed in the literature [15] such as the bow-tie [16] and the oblong [17] transducers in PFB microscopes to obtain directional images with high resolution. In the bow-tie transducer of Fig. 5(a), the effect due to beam steering is not taken into account. In the oblong transducer of Fig. 5(b), the resolution for detecting directionality is reduced for the materials with high LSAW velocity.

We proposed the butterfly-shaped transducer [11] as shown in Fig. 5(c). In this transducer, the circular center electrode is surrounded by a pair of fan-shaped electrodes with an angle ϕ to compose the central and the fan-shaped transducers, respectively. By considering the effects due to beam steering, the centers (O') of the fan-shaped electrodes do not coincide with the center of the transducer. As shown in Fig. 4, the eccentric radius d is determined from the position of the point (A) where the longitudinal wave in water reaches the sample at the incident angle θ_{LSAW} and the LSAW starts to propagate on the boundary with power flow angle $\phi/2$. The eccentric radius d is approximately set to be equal to the distance R in (19) in this paper.

A RF pulse I_{in} excites both the central transducer and the pair of the fan-shaped transducers simultaneously. These transducers also act as receivers and pick up the reflected pulses. The reflected pulse detected by each transducer is passed through a circulator. Then, the two complex $V(z)$ curves are measured by a pulse mode measurement system [18]. In order to apply the microdefocusing method, the two components $V_L(z)$ and $V_I(z)$ are obtained separately from the measured $V(z)$ curves by using the signal processing method as described in the Section V.

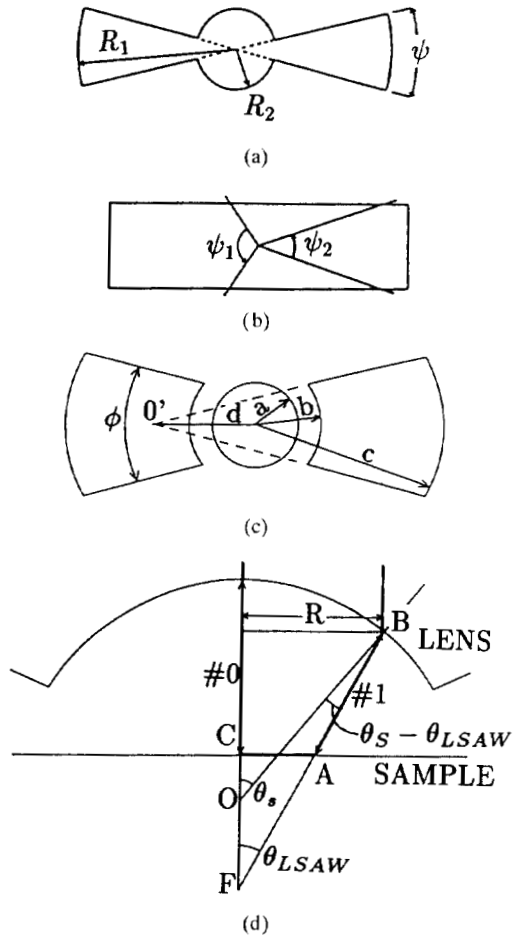

Fig. 5. Illustrations explaining various transducers proposed in literature. (a) Electrode in the Bow-tie type transducer. (b) Electrode in the oblong type transducer. (c) Electrodes in the butterfly transducer and the corresponding paths of acoustic wave propagating through lens, in water, and on the surface of a sample.

V. Signal Processing for Separating $V_L(z)$ and $V_I(z)$

Since the acoustical wave propagates through the lens, water/sample, and back to the lens in sequence, these propagation paths are divided into three phases as shown in Figs. 6(a), 6(b), and 6(c), respectively. In the first and third phases in Figs. 6(a) and 6(c), the diffraction effect should be taken into account.

Let $V_0(z)$ and $V_1(z)$ be the complex responses of the central and fan-shaped transducers to the input amplitudes I_0 and I_1 and also, let the complex coefficients $\{H_{ij}, G_{ji}\}$, $(i = 0, 1; j = L, I)$ represent the transfer system due to the diffraction and the complex coefficients $H_L(z)$ and $H_I(z)$ in Fig. 6(b) the transfer system due to the two components $V_L(z)$ (path #0) and $V_I(z)$ (path #1) in (2) and (3), respectively. Thus, the output $V_0(z)$ and $V_1(z)$ are described as

$$\begin{aligned} V_0(z) &= (I_0 H_{0L} + I_1 H_{1L}) H_L(z) G_{L0} \\ &\quad + (I_0 H_{0I} + I_1 H_{1I}) H_I(z) G_{I0} \\ V_1(z) &= (I_0 H_{0L} + I_1 H_{1L}) H_L(z) G_{L1} \\ &\quad + (I_0 H_{0I} + I_1 H_{1I}) H_I(z) G_{I1}. \end{aligned} \tag{20}$$

In these equations, $H_L(z)$ and $H_I(z)$ are equivalent representations of $V_L(z)$ and $V_I(z)$, respectively.

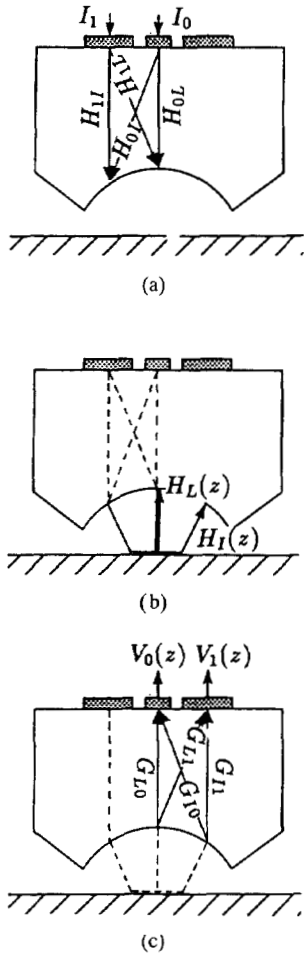

Fig. 6. The propagation paths of waves are divided into three phases. (a) In the lens. (b) In water/sample. (c) In the lens. Complex coefficients $\{H_{ij}, G_{ji}\}$, $(i = 0,1; j = L, I)$, $H_L(z)$, and $H_I(z)$ represent the corresponding transfer systems.

Equation (20) is rewritten in matrix form as

$$\begin{pmatrix} V_0(z) \\ V_1(z) \end{pmatrix} = \begin{pmatrix} C_{L0} & C_{I0} \\ C_{L1} & C_{I1} \end{pmatrix} \begin{pmatrix} V_L(z) \\ V_I(z) \end{pmatrix} \tag{21}$$

by defining the complex constant C_{ji} as

$$C_{ji} = (I_0 H_{0j} + I_1 H_{1j}) G_{ji}. \quad (i = 0,1;\ j = L, I).$$

The complex amplitudes C_{L0}, C_{I0}, C_{L1}, and C_{I1} are determined only by the input amplitudes I_0 and I_1, the shape and the material of the transducer and the acoustical lens, and the frequency. This is because the paths (#0 and #1) in the lens do not change for various defocus ranges near the focal plane. Using (2) and (3), the sampled $V(z)$ curves, namely $V_0(n \cdot \delta z)$ and $V_1(n \cdot \delta z)$ curves, are modeled by

$$\begin{pmatrix} V_0(n \cdot \delta z) \\ V_1(n \cdot \delta z) \end{pmatrix} = \begin{pmatrix} C'_{L0} & C'_{I0} \\ C'_{L1} & C'_{I1} \end{pmatrix} \begin{pmatrix} p_L^n \\ p_I^n \end{pmatrix} \tag{22}$$

where $C'_{ji} = C_{ji} \cdot C_j$, $(i = 0,1;\ j = L, I)$. The complex amplitudes C'_{L0}, C'_{L1}, and C'_{I1} are determined only by the shape and the material of the transducer and the acoustical lens, and the frequency. This is because the paths (#0 and #1) in the lens do not change for various defocus ranges near the focal plane.

Once the resultant coefficients are determined from the transformed data, $V_L(z)$ and $V_I(z)$ of (21) are obtained separately from the measured data $V_0(z)$ and $V_1(z)$.

$$\begin{pmatrix} \widehat{V_I}'(z) \\ \widehat{V_I}'(z) \end{pmatrix} \stackrel{\text{def}}{=} \begin{pmatrix} V_L(z)/C_L \\ V_I(z)/C_I \end{pmatrix} = \frac{1}{\det} \begin{pmatrix} C'_{I1} & -C'_{I0} \\ -C'_{L1} & C'_{L0} \end{pmatrix} \begin{pmatrix} V_0(z) \\ V_1(z) \end{pmatrix} \tag{23}$$

where $\det = C'_{L0}C'_{I1} - C'_{I0}C'_{L1}$. Although the resultant $V'_L(z)$ and $V'_I(z)$ are divided by the factors C_L and C_I, respectively, the gradients ξ_L, ξ_I, η_L, and η_I of (11)–(14) do not depend on these factors. Thus, using the gradients of $\angle V'_L(z)$, $\angle V'_I(z)$, $\ln|V'_L(z)|$, and $\ln|V'_I(z)|$, the acoustic properties (velocity and attenuation factor) of the LSAW component and the longitudinal wave in water are determined from (11)–(16).

Let us consider how to determine the complex amplitudes C'_{L0}, C'_{I0}, C'_{L1}, and C'_{I1} by assuming that $f = 200\ MHz$, $|\delta z| = 0.1\ \mu$m, $v_{\text{LSAW}} \approx 3400\ m/s$ (for fused quartz), and $v_w = 1491$ m/s (for $T = 25°$C) for example. For this purpose, popular parametric spectrum estimation technique [19]–[21] should be applied. However, the angles of the poles p_L and p_I are $-9.64°$ and $-8.66°$, respectively, in the z-plane under these conditions as shown in Fig. 7(a). Thus, the angle difference between these poles in the z-plane is usually very small and it is difficult for the popular parametric spectrum estimation method to accurately separate and determine these poles. Therefore, it is necessary to transform the measured data $V_0(z)$ and $V_1(z)$ into the appropriate forms before applying the spectrum estimation technique for these conditions.

Let us desample these measured data at a period $|\rho \cdot \delta z|(\rho > 1)$, after applying an appropriate low pass filter to $V_0(z)$ and $V_1(z)$. In order to remove the rapid change due to the phase term $\angle p_L$ in (5), let us multiply the resultant desampled $V_0(z)$ and $V_1(z)$ by the factor $\exp(-j2k'_w \cdot \rho \cdot \delta z)$, where k'_w is the assumed wave number in water at the temperature. Then, the angles of the resultant poles p''_L and p''_I in the z-plane are described by $\exp(j2\rho \cdot \delta z(k_w - k'_w))$ and $\exp(j2\rho \cdot \delta z(k_w \cos\theta_{\text{LSAW}} - k'_w))$, respectively. If the value of ρ is 64, $V_0(z)$ and $V_1(z)$ are desampled at a period of 6.4 μm and if $k'_w = k_w$, the angles of the poles p_L and p_I are $0°$ and $62.7°$, respectively, in the z-plane as shown in Fig. 7(b). The resultant pole p''_L is on the real axis in the z-plane. Thus, it is still difficult to estimate the position of such a pole near or on the real axis because the dc component is deleted before applying the popular parametric spectrum estimation method.

Therefore, let us multiply the desampled $V_0(z)$ and $V_1(z)$ not by the factor $\exp(-j2k'_w\rho \cdot \delta z)$ but by the factor $\exp(-j2k'_w\rho \cdot \delta z \cdot \beta))$, where β is a constant $0 \le \beta \le 1$. It is not necessary to set the assumed wave number k'_w as just equal to the true wave number k_w at the temperature because the difference can be corrected as described in the following. This processing is equivalent to the demodulation of a complex signal. From (4) and (5), the angles of the resultant poles p'_L and p'_I in the z-plane are respectively represented by

$$\angle p'_L = 2(k_w - k'_w\beta)\rho \cdot \delta z \tag{24}$$

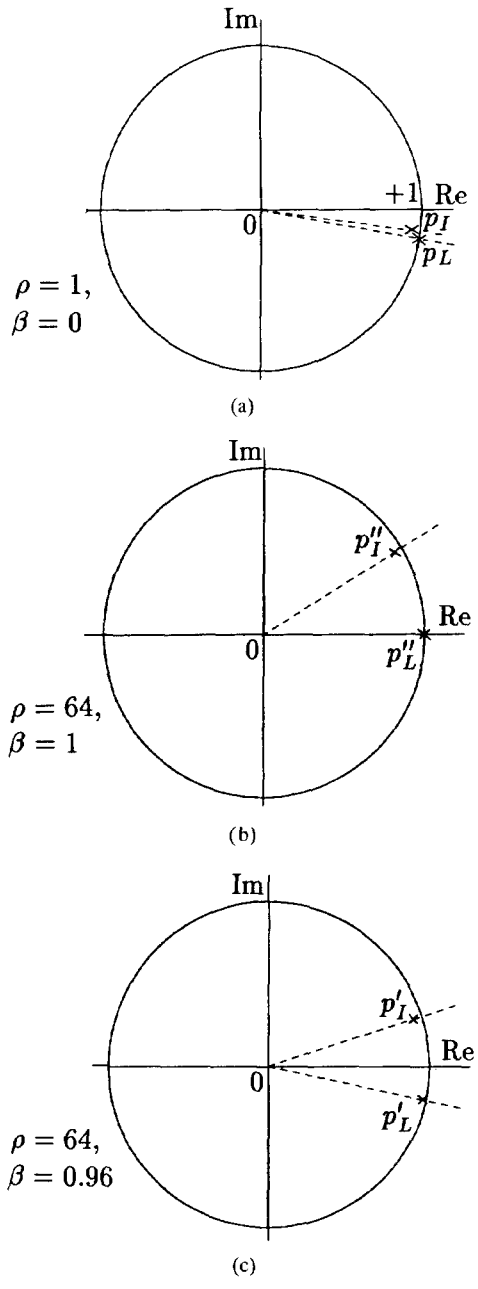

Fig. 7. Illustrations explaining the effect of multiplying $\exp(-j2k'_w\rho \cdot \delta z \cdot \beta)$ when the poles are estimated by popular parametric spectrum estimation methods. (a) $\beta = 0$, $\rho = 1$. (b) $\beta = 1$, $\rho = 64$. (c) $\beta = 0.96$, $\rho = 64$.

and

$$\angle p'_I = 2(k_w \cos\theta_{\mathrm{LSAW}} - k'_w\beta)\rho \cdot \delta z. \tag{25}$$

For the conditions described above, these values are $-24.7°$ and $38.1°$, respectively, as shown in Fig. 7(c) by assuming $k_w = k'_w$, $\rho = 64$, and $\beta = 0.96$.

By applying Prony's method [19] simultaneously to the resultant transformed data of $V_0(n \cdot \rho \cdot \delta z)$ and $V_1(n \cdot \rho \cdot \delta z)$, both poles, p'_L and p'_I, and their complex amplitudes C'_{L0}, C'_{I0}, C'_{L1}, and C'_{I1} are determined by solving twice the linear simultaneous equations derived by minimizing the average power of the difference among the terms in the right-hand and the left-hand sides of (22). Prony's method can model

TABLE I
PARAMETERS OF THE FABRICATED BUTTERFLY TRANSDUCER

TRANSDUCERS:
Material: ZnO Thin-Film (f = 200 MHz).
Radius: a = 0.25 mm, b = 0.35 mm, c = 1.08 mm, d = 0.60 mm.
Angle: $\phi = 30°$
The Point-Focus-Beam Acoustic Lens:
Material: Z-cut sapphire
Rod Length: 7.0 mm.
Radius of curvature: r = 1.25 mm.
Half-Aperture angle: 60°.

a complex sequence as a linear combination of complex exponentials. From the angles of the poles $\hat{p}'_L$ and $\hat{p}'_I$ estimated above, v_w and v_{LSAW} are predetermined by the following equations, which are derived from (6), (8), (23), and (24):

$$\begin{aligned}\widehat{v_w} &= \frac{2\pi f}{\widehat{k_w}} \\ &= \frac{2\pi f}{k'_w\beta + \angle\hat{p}'_L/2\rho \cdot \delta z} \\ &= \frac{4\pi f\rho \cdot \delta z}{4\pi f\rho \cdot \delta z \cdot \beta/v'_w + \angle\hat{p}'_L}\end{aligned} \tag{26}$$

where $v'_w = 2\pi f/k'_w$ is the assumed velocity in water at the temperature and

$$\begin{aligned}\hat{v}_{\mathrm{LSAW}} &= \frac{\hat{v}'_w}{\sin\theta_{\mathrm{LSAW}}} \\ &= \frac{\hat{v}'_w}{\sin(\cos^{-1}(\beta k'_w/k_w - \angle\hat{p}'_I/2k_w\rho \cdot \delta z))}.\end{aligned} \tag{27}$$

Once the coefficients C'_{L0}, C'_{I0}, C'_{L1}, and C'_{I1} are determined in advance using the procedure above, $\hat{V}'_L(z)$ and $\hat{V}'_I(z)$ are separately obtained from the observed outputs $V_0(z)$ and $V_1(z)$ of the proposed transducer using (23), and then the acoustic properties are determined from (11)–(16).

VI. EXPERIMENTS AND THE RESULTS

Based on the design rules described in Section IV, the parameters of the butterfly transducer were determined so as to detect an LSAW component with a phase velocity in the range of 2100 m/s to 5500 m/s. Table I shows the parameters of the fabricated butterfly transducer, which is employed in the following experiments.

RF burst pulses with a width of 500 ns are applied to both transducers through the attenuators and the circulators in Fig. 4. The repetition rate of the RF burst pulses is 0.1 ms. The attenuation level for the inputs of the central transducer and the surrounding transducers are 10 dB and 0 dB, respectively. $V_0(z)$ and $V_1(z)$ are obtained by measuring the resultant voltage after gating and amplifying the output signal of the corresponding transducer while the z-stage is moved along the z-axis by the step $|\delta z|$ of 0.1 μm. The employed frequency f is 200 MHz.

Fig. 8 shows the measured $V_0(n \cdot \delta z)$ and $V_1(n \cdot \delta z)$ for a sample of fused quartz in the defocus range from $z = 0$ to $z = 500$ μm. In order to remove the rapid change of the phase, each value is multiplied by $\exp(-j2k'_w \cdot \delta z \cdot \beta)$, $(\beta = 0.96)$, where

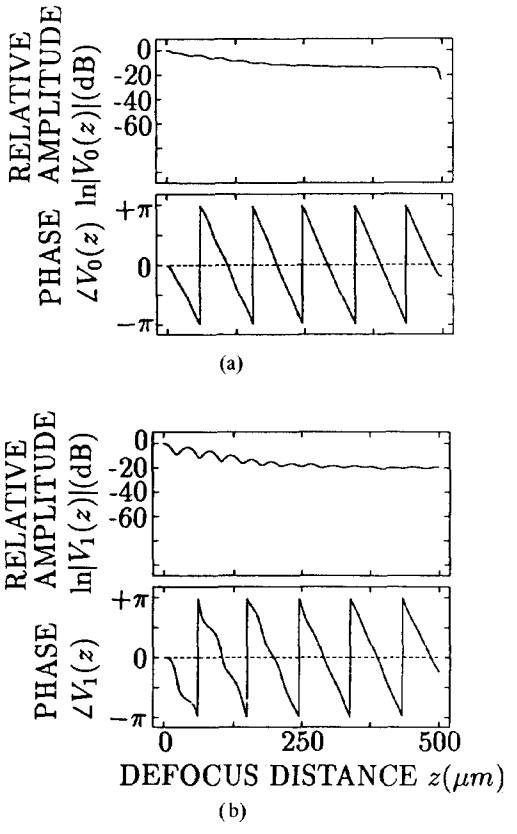

Fig. 8. The characteristics of the $V_0(z)$ and $V_1(z)$ measured in the defocus range from 0 μm to 500 μm.

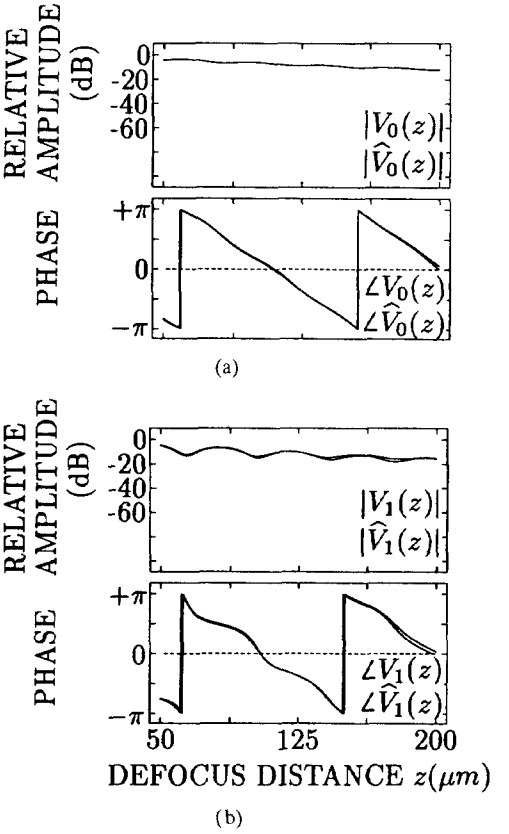

Fig. 9. The characteristics of the measured $V_0(z)$ and $V_1(z)$ and the estimated $\hat{V}_0(z)$ and $\hat{V}_1(z)$.

k'_w is obtained from the measured temperature. By applying the nonlinear least square optimization technique [22] using the parameters obtained by Prony's method as initial values, satisfactory results are obtained because both the measured and the modeled data coincide well in phase and amplitude. Fig. 9 shows the measured $V_0(n \cdot \delta z)$ and $V_1(n \cdot \delta z)$ and the estimated $\hat{V}_0(n \cdot \delta z)$ and $\hat{V}_1(n \cdot \delta z)$ modeled in (22) in the defocus range from $z = 50$ μm to $z = 200$ μm.

In the nonlinear least square optimization procedure, the following normalized error function ζ is minimized with respect to the poles p'_L and p'_I and the complex coefficients C'_{L0}, C'_{L1}, C'_{I0}, and C'_{I1} (see (28) at the bottom of the page) where n_1 and n_2 represent the points for the beginning $(z = z_1 = \rho \cdot \delta z \cdot n_1)$ and the end $(z = z_2 = \rho \cdot \delta z \cdot n_2)$ of the defocusing range, respectively.

Fig. 10 shows the minimized error function ζ obtained from the data of the various defocus ranges $[z_1, z_2]$ of $V_0(z)$ and $V_1(z)$ in Fig. 8(a). When the defocus range $[z_1, z_2]$ involves a region less than 50 μm, the values ζ of the resultant error function takes large values for each defocus distance $D_Z = |z_2 - z_1|$. Thus, it is found for these experiments that the models of (2) and (3) do not hold for the data in defocus regions near the focal plane ($z = 50$ μm).

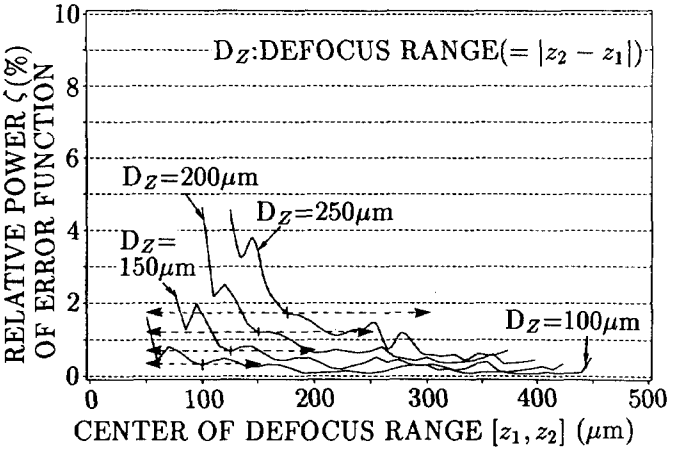

Fig. 10. The minimized error function ζ obtained for the data of the various defocus range $[z_1, z_2]$ of $V_0(z)$ and $V_1(z)$ in Fig. 8.

In the experiments, therefore, the defocus region employed to determine the complex coefficients is from 50 μm to 200 μm. Fig. 11(a) shows the positions of the resultant es-

$$\zeta = \frac{\sum_{n_1}^{n_2} \left| V_0(n\rho\delta z) - \hat{V}_0(n\rho\delta z) \right|^2 + \sum_{n_1}^{n_2} \left| V_1(n\rho\delta z) - \hat{V}_1(n\rho\delta z) \right|^2}{\sum_{n_1}^{n_2} |V_0(n\rho\delta z)|^2 + \sum_{n_1}^{n_2} |V_1(n\rho\delta z)|^2} \tag{28}$$

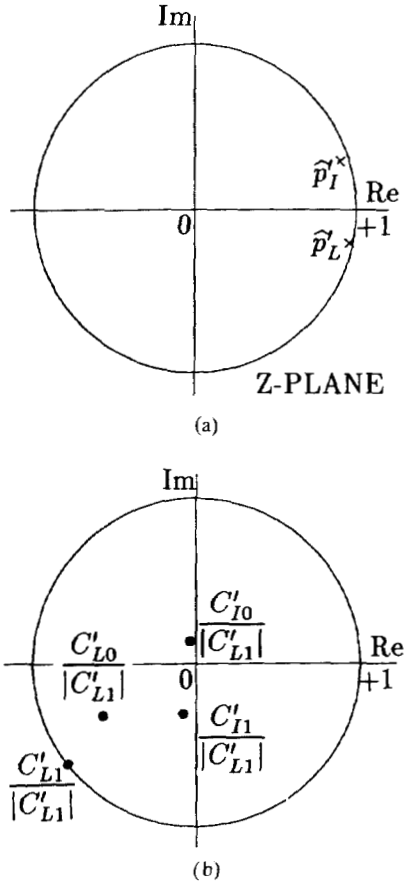

Fig. 11. (a) Positions of the estimated poles $\widehat{p'}_I$ and $\widehat{p'}_L$ in the z-plane. (b) Positions of the obtained complex coefficients C'_{L0}, C'_{I0}, and C'_{I1} normalized by the magnitude $|C'_{L1}|$.

timated poles $\widehat{p'}_I$ and $\widehat{p'}_L$ in the z-plane. Fig. 11(b) shows the positions of the obtained complex coefficients C'_{L0}, C'_{L1}, C'_{I0}, and C'_{I1} of (22), which are normalized by the magnitude $|C'_{L1}|$.

By substituting the resultant complex coefficents into the right-hand side of (23), the two components $\widehat{V}'_L(z)$ and $\widehat{V}'_I(z)$ are obtained near the focal plane separately from the measured $V_0(z)$ and $V_1(z)$ as shown in Figs. 12(a) and (b), respectively. Each term is multiplied by $\exp(-j2k'_w \cdot \delta z \cdot \beta)$, $(\beta = 1)$. The phase characteristics are represented by almost straight lines, which means that both components $V_I(z)$ and $V_L(z)$ are successfully obtained from the transducer outputs $V_0(z)$ and $V_1(z)$. The reason why the phase value $\angle V_L(z)$ in Fig. 12(a) does not equal zero is due to the difference between k_w determined from the measured data and k'_w obtained from the temperature. By determining the average gradient ξ_L and ξ_I of $\angle \widehat{V}'_L(z)$ and $\angle \widehat{V}'_I(z)$ in the defocusing range from 50 μm to 125 μm, the longitudinal phase velocity v_w in water and the phase velocity v_{LSAW} of fused quartz are obtained as $v_w = 1497$ m/s and $v_{\mathrm{LSAW}} = 3442$ m/s, respectively, which are reasonable values. Thus, the principle of the microdefocusing method is successfully proved by the experiments.

It is important to evaluate the defocus range $[z_1, z_2]$ for the determination of the gradients and the velocities. Fig. 13 shows the phase velocity v_{LSAW} of the LSAW and the longitudinal velocity v_w in water estimated from the various ranges of the resultant $V_L(z)$ and $V_I(z)$ in Fig. 12. It is

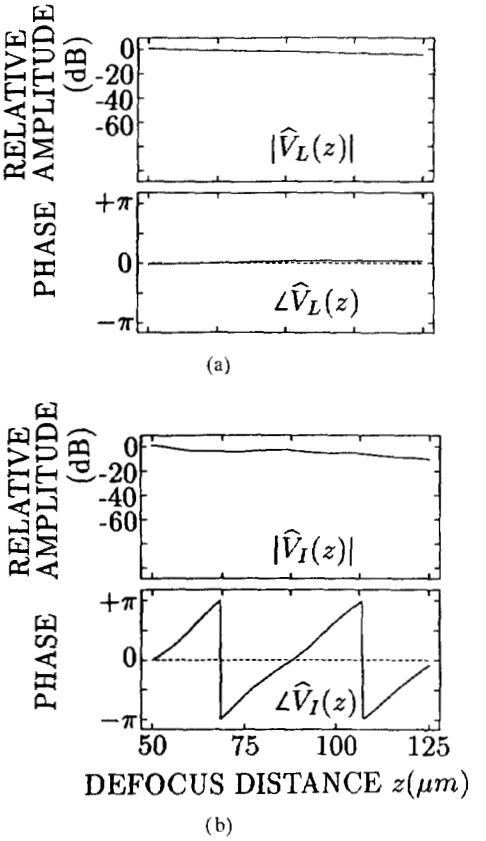

Fig. 12. Two components $\widehat{V}_L'(z)$ and $\widehat{V}_I'(z)$ obtained separately from the $V_0(z)$ and $V_1(z)$ measured in the defocus range from 50 μm to 125 μm.

necessary for the reasonable determination of the velocity to use the data in the defocus distance greater than 40 μm, which is almost equal to the interference period $\Delta z (= 36.7\ \mu\mathrm{m})$ in (9).

VII. Conclusion

This paper has described a new method to obtain acoustic properties by analyzing the transducer outputs $V(z)$, which are measured within the microdefocusing region near the focal plane. The proposed method determines the acoustic properties of a sample from the gradients of the $V_L(z)$ and $V_I(z)$ curves without applying any periodic analysis. In order to obtain these components $V_L(z)$ and $V_I(z)$ separately, a new-type of transducer called the "butterfly transducer," which has two sets of electrodes is introduced and a signal processing for determining the $V_L(z)$ and $V_I(z)$ components from the resultant outputs $V_0(z)$ and $V_1(z)$ of the transducer is developed. Some experiments have performed to confirm the principle developed in this study for obtaining $V_L(z)$ and $V_I(z)$ from the outputs $V_0(z)$ and $V_1(z)$ of the transducer.

When the propagation attenuation of a sample is large and/or the velocity value of the LSAW is large, sufficient defocus distance necessary for current $V(z)$ analysis cannot be attained. Though the experimental results are shown only for a fused quartz in this paper, the proposed method will be applied to overcome these problems. It is also expected that a practical acoustic microscope system for quantitative imaging will be constructed based on the proposed principle and it will

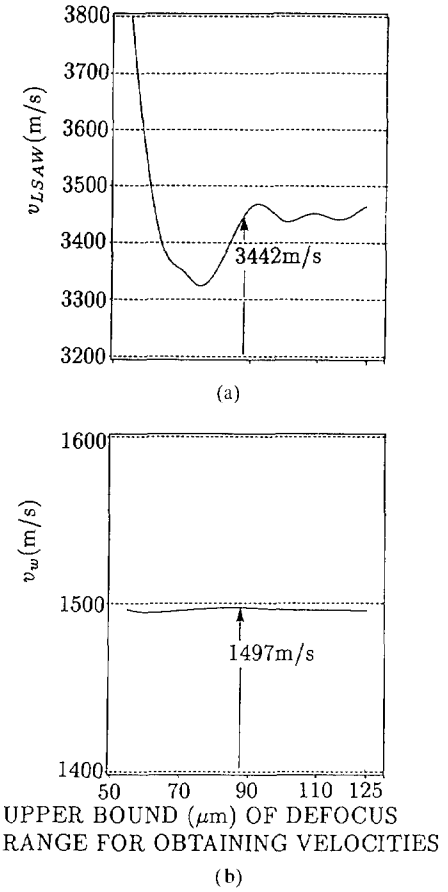

Fig. 13. The phase velocity v_{LSAW} of the LSAW and the longitudinal velocity v_w in water estimated from the various defocus ranges $[z_1, z_2]$ of the resultant $\hat{V}_L'(z)$ and $\hat{V}_l'(z)$ in Fig. 12, where the lower bound z_1 of the range is 50 μm.

play a significant role in fields of the acoustical imaging and microspectroscopy.

ACKNOWLEDGMENT

The authors wish to thank Mr. Toshihiro Wakahara for his assistance of the experiments and Mr. Derek Iwamoto of our laboratory for his preparation of the manuscript.

REFERENCES

[1] R. A. Lemons and C. F. Quate, "A scanning acoustic microscope, in *Proc. 1973 IEEE Ultrason. Symp.*, 1973, pp. 18–20.
[2] C. F. Quate, A. Atalar, and H. K. Wickramasinghe, "Acoustic microscope with mechanical scanning—A review," *Proc. IEEE*, vol. 67, pp. 1092–1114, Aug. 1979.
[3] A. Atalar, "An angular-spectrum approach to contrast in reflection acoustic microscope," *J. Appl. Phys.*, vol. 49, pp. 5130–5139, Oct. 1978.
[4] R. D. Weglein, "A model for predicting acoustic material signatures," *Appl. Phys. Lett.*, vol. 34, pp. 179–181, Feb. 1979.
[5] W. Parmon and H. L. Bertoni, "Ray interpretation of the material signature in the acoustic microscope," *Electron. Lett.*, vol. 15, pp. 684–686, Oct. 1979.
[6] A. Atalar, "A physical model for acoustic signatures," *J. Appl. Phys.*, vol. 50, pp. 8237–8239, Dec. 1979.
[7] R. D. Weglein, "Rayleigh wave absorption via acoustic microscopy," *Electron. Lett.*, vol. 18, pp. 20–21, Jan. 1982.
[8] J. Kushibiki, K. Horii, and N. Chubachi, "Velocity measurement of multiple leaky waves on Germanium by line-focus-beam acoustic microscope using FFT," *Electron. Lett.*, vol. 19, pp. 404–405, May 1983.
[9] J. Kushibiki, Y. Mastumoto, and N. Chubachi, "Attenuation measurement of leaky waves on Germanium by acoustic line-focus-beam," *Electron. Lett.*, vol. 19, pp. 512–514, July 1983.
[10] J. Kushibiki and N. Chubachi, "Material characterization by line-focus-beam acoustic microscope," *IEEE Trans. Sonics Ultrason.*, vol. SU-32, pp. 189–212, Mar. 1985.
[11] N. Chubachi, H. Kanai, T. Sannomiya, and T. Wakahara, "Acoustic microscope for measuring acoustic properties by microdefocusing method," in *Acoustical Imaging*, H. Ermert and H.-P. Harjes, Eds. New York: Plenum, 1991. (Also presented in 19th Symp. Acoust. Imaging, Ruhr-Universität Bochum, Germany, Apr. 1991.
[12] M. Greenspan and C. E. Tschiegg, "Speed of sound in water by a direct method," *J. Res. Nat. Bur. Stand*, vol. 59, pp. 249–254, Oct. 1957.
[13] H. Kanai, N. Chubachi, and H. Suzuki, "A method to evaluate accurqcy of FFT-based periodicity analysis for short length signal in low SNR," in *Proc. IEEE 1992 Int. Conf. Acoust., Speech, Signal Processing*, Mar. 1992, pp. V45–V48.
[14] J. M. M. Pinkerton, "The absorption of ultrasonic waves in liquids and its relation to molecular constitution," *Proc. Phys. Soc.*, vol. B20, Feb. 1949, pp. 129–141.
[15] J. A. Hildebrand and L. K. Lam, "Directional acoustic microscope for observation of elastic anisotropy," *Appl. Phys. Lett.*, vol. 42, No. 5, pp. 413–415, Mar. 1983.
[16] D. A. Davids and H. L. Bertoni, "Bow-tie transducers for measurement of anisotropic materials in acoustic microscopy," in *Proc. IEEE Ultrason. Symp.*, 1986, pp. 735–740.
[17] N. Chubachi, *et al.*, "Acoustic images observed by directional PFB microscope," in *Proc. 18th Symp. Acoust. Imaging*, 1989.
[18] Y. Sugawara, J. Kushibiki, and N. Chubachi, "Performance of concave transducers in acoustic microscopy," in *Proc. 1988 IEEE Ultrason. Sympo.*, 1988, pp. 751–756.
[19] J. D. Markel and A. H. Gray, Jr., *Linear Prediction of Speech*. Heidelburg, Germany: Springer, Ch. 2, 1976.
[20] S. L. Marple, Jr., *Digital Spectral Analysis with Applications*. Englewood Cliffs, NJ: Prentice Hall, 1987.
[21] S. M. Kay, *Modern Spectral Estimation Theory and Application*. Englewood Cliffs, Prentice Hall, 1988.
[22] D. Marquardt, "An algorithm for least-squares estimation of nonlinear parameters," *SIAM J. Appl. Math.*, vol. 11, pp. 431–441, 1963.

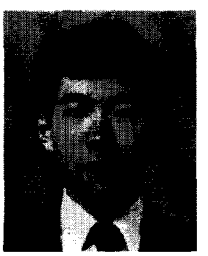

Hiroshi Kanai (A'89–M'91) was born in Matsumoto, Japan on November 29, 1958. He received the B.E. degree from Tohoku University, Sendai, Japan, in 1981, and the M.E. and the Dr. Eng. degrees, also from Tohoku University, in 1983 and in 1986, both in electrical engineering.

From 1986 to 1988 he was with the Education Center for Information Processing, Tohoku University, as a Research Associate. From 1990 to 1992, he was a Lecturer with the Faculty of Engineering, Tohoku University. Since 1992 he has been a Associate Professor at the Department of Electrical Engineering, Faculty of Engineering, Tohoku University. His present interest is in digital signal processing and its application on the acoustical, ultrasonic, and electrical measurements.

Dr. Kanai is a member of the Acoustical Society of Japan, the Institute of Electronics, Information, and Communication Engineering of Japan, the Japan Society of Mechanical Engineers, the Japan Society of Ultrasonics in Medicine, Japan Society of Medical Electronics and Biological Engineering, and the Institute of Electrical Engineers of Japan.

Noriyoshi Chubachi (M'83) was born in Kokura, Japan, on October 5, 1933. He received the B.S., M. S., and Ph.D degrees in electrical engineering from Tohoku University, Sendai, Japan, in 1956 and in 1962, and 1965, respectively.

In 1965, he joined the Research Institute of Electrical Communication, Tohoku University, where he was an Associate Professor from 1966 to 1978. Since 1979 he has been a Professor at the Department of Electrical Engineering, Tohoku University. From 1982 to 1983 he was a visiting Professor of Electrical and Computer Engineering, University of California, Santa Barbara, CA. He has worked on ultrasonic transducers and delay lines, surface acoustic devices, acoustoelectronics, piezoelectric materials, accoustic microscopy, and related problems.

Dr. Chubachi is a member of the Institute of Electronics and Communication Engineers of Japan, the Society of Japanese Applied Physics, the Acoustical Society of Japan, the Japan Society of Ultrasonics in Medicine, the Japan Society for Nondestructive Inspection, the Japan Society of Medical Electronics and Biological Engineering, the Japan Society of Mechanical Engineers, and the Institute of Electrical Engineers of Japan. He served as chairman, Tokyo chapter of IEEE UFFC Society, from 1987 to 1988.

Toshio Sannomiya was born in Miyagi Prefecture, Japan, on October 3, 1938. He graduated from the Sendai Radio High School in 1959.

From 1959 to 1978, he was with the Research Institute of Electrical Communication, Tohoku Univesity, Sendai, Japan. Since 1979, he has been at the Department of Electrical Engineering, Faculty of Engineering, Tohoku University. He has engaged in the studies of ultrasonic transducers, ultrasonic measurements, and acoustic microscopy.

Mr. Sannomiya is a member of the Acoustical Society of Japan, and the Japan Society of Ultrasonics in Medicine.